GMR
The Original

DEFECT-SPARSE 2D CARBON IN EPOXY POWDER COATINGS: PORE CONTROL AND EIS DURABILITY

Mahesh Chaudhari*

*Email: maheshchaudhari848@gmail.com

ABSTRACT
A thermoset powder-coating platform was formulated by integrating a defect-sparse two-dimensional carbon nanoadditive into an epoxy matrix to suppress microporosity, enhance network formation, and improve long-term barrier function against chloride brines. The nanoadditive was manufactured via benign liquid-phase shear exfoliation with polymeric stabilization, converted to a dry powder, dispersed at ultra-low loadings, electrostatically deposited onto steel, and oven-cured to yield dense polymer films representative of industrial powder-coating practice.Polymer/coating diagnostics spanning SEM (microstructure), FTIR/Raman (chemical signatures), DSC (cure onset and heat transport), and adhesion by pull-off testing were coupled to electrochemical evaluations (EIS with equivalent-circuit modeling and Tafel analysis) to establish processing–structure–property relationships in the barrier film. Optimized low-loading formulations reduced cavity/micropore prevalence, preserved interfacial adhesion after aggressive salt exposure, and sustained high low-frequency impedance over multi-week immersion, reflecting improved coating resistance and mitigated charge-transfer at the coating–metal interface. Cure-kinetic and thermal evidence indicate that the nanoadditive subtly advances epoxy ring-opening and promotes levelling-driven porosity reduction, complementing its physical tortuosity effect at sub-0.1 wt% concentrations. Together, these polymer-centric findings define a scalable, chromate-free route to epoxy powder barrier coatings in which 2D carbon modulates porosity, curing, and electrochemical response to deliver durable corrosion protection.

Index Terms—Graphene, epoxy powder coating, corrosion protection, electrochemical impedance spectroscopy, adhesion strength, thermal conductivity.

I. INTRODUCTION

Metal corrosion represents one of the most significant economic challenges facing industrial societies, with annual global costs estimated in trillions of dollars across infrastructure, transportation, and manufacturing sectors [1]. The fundamental approach to corrosion mitigation involves creating effective barriers between metallic substrates and corrosive environments, with organic coatings emerging as the most versatile and widely implemented solution due to their flexibility, adaptability, and cost-effectiveness [2]. Among various coating technologies, powder coatings have gained substantial market share in recent decades, offering distinct advantages over traditional liquid formulations by eliminating volatile organic compounds, reducing waste, and providing enhanced durability in humid conditions [3].

Epoxy resins constitute a predominant class of thermosetting polymers employed in protective coatings, valued for their exceptional mechanical properties, chemical resistance, and strong adhesion to metallic substrates [4]. However, the corrosion protection performance of epoxy coatings is frequently compromised by inherent structural limitations, including incomplete crosslinking between epoxy and curing agent molecules, susceptibility to crack propagation, and the formation of microscopic defects during the curing process [5]. These structural imperfections create diffusion pathways that allow corrosive species, particularly chloride ions, to penetrate the coating and reach the underlying metal substrate, ultimately leading to coating failure and substrate corrosion
[6].

The incorporation of nanoscale fillers has emerged as a promising strategy to enhance the barrier properties of epoxy coatings by modifying their microstructure and impeding the transport of corrosive agents [7]. Various nanomaterials, including metal oxides, clay minerals, and carbon-based structures, have been investigated for this purpose. For instance, Samad et al. [8] demonstrated that zinc oxide nanoparticles at 2 wt% loading effectively reduced surface defects and improved the corrosion resistance of epoxy coatings. Similarly, Xia et al. [9] developed SiO_2-MoS_2 core-shell nanofillers that enhanced both anticorrosion performance and mechanical properties through improved interfacial interactions within the epoxy matrix.

Carbon nanomaterials, particularly those with twodimensional geometries, offer exceptional potential as reinforcing fillers in polymer coatings due to their high aspect ratios, large specific surface areas, and outstanding barrier properties [10]. Graphene, consisting of a single atomic layer of carbon atoms arranged in a hexagonal lattice, represents the ultimate two-dimensional carbon material with theoretical impermeability to even the smallest atoms, including helium [11]. This exceptional barrier characteristic, combined with high mechanical strength and chemical stability, positions graphene as an ideal nanofiller for enhancing the corrosion protection performance of polymeric coatings [12].

The practical implementation of graphene in coating systems faces several significant challenges, primarily related to the quality of the graphene material and its dispersion within the polymer matrix. Conventional graphene production methods often introduce structural defects that compromise barrier properties, while the strong interlayer π-π interactions promote agglomeration, leading to stress concentration points and reduced coating performance [13]. Various strategies have been developed to address these issues, including chemical functionalization and non-covalent modification with surfactants or polymers to improve dispersion stability and interfacial compatibility [14].

Despite extensive research on graphene-enhanced liquid coatings, investigations into graphene-reinforced powder coatings remain relatively limited, particularly concerning the fundamental mechanisms through which graphene improves coating performance at ultralow loadings [15]. Powder coating systems present unique challenges and opportunities compared to their liquid counterparts, as the coating formation process involves distinct stages of powder deposition, melting, leveling, and crosslinking [16]. Understanding how graphene influences each of these stages is crucial for optimizing coating formulations and manufacturing processes.

This comprehensive study establishes a multifunctional platform for developing high-performance epoxy powder coatings through the incorporation of defect-sparse graphene produced via environmentally benign liquid-phase shear exfoliation. The research systematically investigates the effects of graphene loading on coating microstructure, curing behavior, thermal properties, adhesion strength, and electrochemical performance. By correlating material characteristics with functional properties across multiple length scales, this work provides fundamental insights into the reinforcement mechanisms of two-dimensional carbon nanomaterials in thermoset powder coatings and establishes design principles for next-generation protective coating systems.

II. MATERIALS AND EXPERIMENTAL METHODS

A. Raw Materials and Substrate Preparation

The experimental materials employed in this investigation included natural graphite powder (325 mesh, Shanghai Aladdin Biochemical Technology Co., Ltd.) as the precursor for graphene production. Polyvinyl alcohol (PVA) with a hydrolysis degree of 98.0%–98.8% and viscosity of 62.0–72.0 mPa·s (Sinopharm Chemical Reagent Co., Ltd.) served as the stabilizer during graphene exfoliation. Commercial epoxy powder coating material was supplied by Zhongshan Hizinco Materials Science & Technology Co., Ltd., representing a typical industrial formulation for corrosion protection applications. Q235 carbon steel plates (150 mm × 70 mm × 0.8 mm) obtained from Jiangsu Guoqiang Galvanizing Industrial Co., Ltd. were utilized as substrates for coating deposition and evaluation.

Substrate preparation followed standardized procedures to ensure consistent surface conditions and promote optimal coating adhesion. The steel plates underwent thorough degreasing using analytical grade ethanol to remove organic contaminants and oils, followed by rinsing with distilled water and drying under ambient conditions. This surface treatment protocol eliminated variables associated with substrate contamination while maintaining the native oxide layer that contributes to initial coating adhesion through secondary bonding interactions [17].

B. Graphene Production via Shear Exfoliation

The graphene production methodology employed a modified liquid-phase shear exfoliation approach based on established principles of high-shear processing in optimized solvent systems [18]. The experimental procedure initiated with the preparation of a PVA stabilizer solution by dissolving

0.5 g of PVA powder in deionized water under magnetic agitation, followed by heating to 90–95°C for 30 minutes to achieve complete dissolution. Concurrently, 5 g of graphite powder was pre-dispersed in ethanol to facilitate subsequent exfoliation.

The graphite-ethanol suspension was combined with the PVA solution to create a 600 mL water-ethanol mixture with optimized volume ratio determined through preliminary screening experiments. High-shear exfoliation was performed using a commercial dispersing emulsifier (FLUKO FA40, China) operated at 11,000 rpm for 1 hour in an ice water bath to maintain temperature control and prevent thermal degradation. The processing protocol included intermittent cooling periods (30 minutes operation followed by 15 minutes rest) to mitigate overheating effects that could compromise graphene quality or induce structural defects.

Following exfoliation, the resulting graphene/graphite suspension underwent centrifugal separation at 500 rpm (26g) for 45 minutes to sediment unexfoliated graphite particles, yielding a stable graphene dispersion. For powder coating applications, the graphene dispersion was concentrated via ultracentrifugation at 10,000 rpm (10,744g) for 30 minutes to produce a graphene sediment, which was subsequently converted to dry powder through freeze-drying (LGJ-12, China) and gentle mechanical crushing to preserve the nanomaterial structure.

C. Coating Fabrication and Processing

The fabrication of graphene-reinforced epoxy powder coatings employed a straightforward dry blending approach to ensure compatibility with industrial powder coating processes. Precisely weighed quantities of graphene powder were mixed with epoxy powder through mechanical stirring to achieve homogeneous distributions at targeted loading levels of 0.0125, 0.025, and 0.05 wt%. These ultralow concentrations were selected to evaluate the efficacy of graphene at loadings relevant to commercial applications while minimizing material costs and potential processing challenges.

Coating deposition utilized electrostatic spraying (WAGNER PEM-X1, Germany) to apply the powder mixtures onto the prepared steel substrates, creating uniform layers with controlled thickness. The electrostatic deposition process leveraged the triboelectric charging of powder particles to ensure efficient transfer and adhesion to the grounded steel substrates. Following deposition, the coated panels underwent thermal curing in a convection oven (YIHENG DHG-9055A, China) at 180°C for 10 minutes, representing standard industrial curing conditions for epoxy powder coatings.

The experimental matrix included four distinct coating formulations: neat epoxy (designated EP) serving as the control, and three graphene-reinforced variants containing
0.0125 wt% ($Gr_{0.0125}$/EP), 0.025 wt% ($Gr_{0.025}$/EP), and 0.05 wt% ($Gr_{0.05}$/EP) graphene loading. This systematic variation enabled comprehensive evaluation of composition-property relationships across the investigated parameter space.

D. Materials Characterization Techniques

The graphene materials underwent extensive characterization to establish their structural and chemical properties. Ultraviolet-visible spectroscopy measured dispersion concentrations and optimized solvent compositions based on absorbance at 660 nm [19]. Atomic force microscopy determined graphene thickness and layer number statistics through topographic imaging on mica substrates. X-ray diffraction analysis compared the crystalline structures of graphite precursors and exfoliated graphene powders, while laser diffraction particle size analysis quantified aggregation behavior. Scanning electron microscopy provided high-resolution imaging of powder morphologies and coating microstructures, with particular emphasis on defect distribution and filler dispersion. Fourier-transform infrared spectroscopy identified chemical functional groups and potential interactions between graphene and the epoxy matrix. Raman spectroscopy evaluated structural perfection through the D/G band intensity ratio and detected charge transfer phenomena [20].

Thermal analysis employed differential scanning calorimetry to investigate curing kinetics and thermal transport properties. The curing behavior assessment included determination of onset temperatures, reaction enthalpies, and analysis of melting endotherms to derive relative thermal conductivity enhancements [21]. All characterization measurements followed standardized protocols with appropriate replication to ensure statistical significance.

TABLE I: Coating Formulation Designations and Composition Details

Sample Designation	Graphene Content (wt%)	Epoxy Content (wt%)	Total Mass (g)	Graphene Mass (mg)
EP	0.00	100.00	500.0	0.0
Gr0.0125/EP	0.0125	99.9875	500.0	62.5
Gr0.025/EP	0.0250	99.9750	500.0	125.0
Gr0.05/EP	0.0500	99.9500	500.0	250.0

E. Electrochemical and Performance Evaluation

Corrosion protection performance assessment employed multiple complementary techniques to establish comprehensive structure-property relationships. Electrochemical impedance spectroscopy measurements utilized a three-electrode configuration with the coated steel as working electrode, platinum counter electrode, and saturated Ag/AgCl reference electrode. Testing occurred in 3.5% NaCl solution over 30-day immersion periods, with spectra acquired from 0.01 Hz to 100 kHz at the open circuit potential with 10 mV perturbation amplitude.

Equivalent circuit modeling fitted the impedance data using established physical models representing coating capacitance, pore resistance, double-layer effects, and charge transfer processes [22]. Tafel polarization measurements complemented the impedance analysis by determining corrosion current densities and potentials after extended immersion, providing additional quantitative metrics of coating protective efficacy.

Accelerated corrosion testing followed ASTM B117 standards through salt spray exposure in 5% NaCl fog at 35°C, with periodic visual inspection and photographic documentation of corrosion progression, particularly at intentionally introduced scratches that created defined defect sites. Adhesion performance evaluation employed pull-off testing according to standardized protocols, measuring bond strength before and after salt spray exposure to assess coating durability under aggressive conditions.

Mechanical property assessment included cross-sectional hardness measurements and flexibility evaluation through conical mandrel bending tests. Thermal stability investigation utilized thermogravimetric analysis to determine decomposition temperatures and residual char contents, providing insights into the influence of graphene on coating thermal performance.

Coating Performance

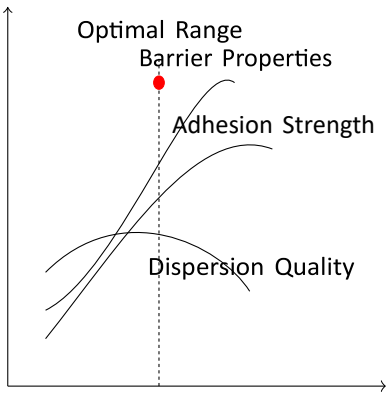

Fig. 1: Conceptual representation of coating performance as a function of graphene loading, illustrating the optimal composition range for balanced properties.

III. RESULTS AND DISCUSSION: NANOMATERIAL CHARACTERISTICS

A. Graphene Production Optimization and Structural Properties

The liquid-phase shear exfoliation process successfully produced high-quality graphene with minimal structural defects, as confirmed by comprehensive materials characterization. Optimization of solvent composition revealed that water-ethanol mixtures with 6:4 volume ratio provided optimal exfoliation efficiency, yielding graphene concentrations of approximately 0.15 mg/mL based on UV-vis absorbance calibration. This solvent composition corresponds to a surface tension of 31 mN/m, which represents an optimal balance between graphene-solvent interaction energy and viscosity for efficient exfoliation while maintaining dispersion stability [23].

Atomic force microscopy analysis demonstrated that the exfoliated graphene sheets exhibited thicknesses between 1.5 and 2.0 nm, corresponding to approximately 5-6 graphene layers based on the theoretical thickness of 0.34 nm per layer. This multilayer structure preserves the essential twodimensional character while providing sufficient mechanical integrity to withstand processing stresses during powder production and coating fabrication. The lateral dimensions of the exfoliated sheets ranged from 0.5 to 3.0 m, yielding aspect ratios sufficient to create tortuous diffusion pathways within the coating matrix while remaining compatible with powder coating application equipment.

X-ray diffraction analysis confirmed successful exfoliation through the characteristic attenuation of the (002) graphite peak at 26.5°. While the graphite precursor exhibited a sharp, intense diffraction peak indicative of well-ordered crystalline structure, the exfoliated graphene powder showed substantially reduced peak intensity and slight broadening, consistent with decreased crystallite size and layer stacking disorder. The persistence of a weak (002) peak suggests the presence of some residual multilayer graphite particles that survived the centrifugation separation, though at concentrations low enough to not significantly impact coating performance.

Particle size distribution analysis provided quantitative evidence of improved dispersion state in the graphene powder compared to the graphite precursor. The graphite powder showed a bimodal distribution with primary peaks below 50 m corresponding to individual particles and secondary peaks around 450 m representing large agglomerates. In contrast, the graphene powder exhibited a monomodal distribution centered below 50 m with no significant population above 100 m, confirming effective deagglomeration through the exfoliation and freeze-drying process. This improved dispersion characteristics critical for achieving uniform distribution within the epoxy powder matrix.

B. Chemical Structure and Surface Functionality

Fourier-transform infrared spectroscopy revealed the chemical signatures of the PVA stabilizer on the graphene surfaces, with the exfoliated material showing enhanced absorption in the O-H stretching region around 3460 cm^{-1} compared to the pristine graphite. This observation confirms the presence of PVA molecules adsorbed on the graphene surfaces through non-covalent interactions, predominantly CH-π bonding between the polymer alkyl chains and the graphene π-electron system. The PVA stabilizer plays a dual role during processing: preventing reagglomeration through steric repulsion in the liquid dispersion and facilitating compatibility with the epoxy matrix during coating formation.

Raman spectroscopy provided definitive evidence of the high structural quality of the exfoliated graphene, with the intensity ratio of D to G bands (I_D/I_G) measuring approximately 0.08. This exceptionally low defect ratio indicates minimal basal plane damage during the shear exfoliation process, preserving the intrinsic barrier properties of the graphene sheets. The G band position shifted from 1583 cm^{-1} for graphite to 1572 cm^{-1} for the exfoliated graphene, suggesting electron transfer from the PVA stabilizer to the graphene sheets through interfacial interactions.

For the composite powder formulations, FTIR analysis detected weak but identifiable signatures of graphene in the $Gr_{0.025}$/EP sample, particularly a subtle absorption around 1640 cm^{-1} attributable to C=C stretching vibrations. This observation confirms the homogeneous distribution of graphene within the epoxy powder matrix at the macroscopic scale. Similarly, Raman spectroscopy of the composite powder revealed a faint G band at 1572 cm^{-1}, providing additional evidence of successful integration without significant agglomeration or phase separation.

The preservation of graphene's structural integrity combined with the presence of compatible surface functionality represents an optimal balance for reinforcement applications in thermoset coatings. The defect-sparse basal planes maintain impermeability to corrosive species, while the surface-adsorbed PVA promotes dispersion stability and interfacial adhesion without introducing covalent defects that could compromise barrier performance or electrical insulation properties.

IV. RESULTS AND DISCUSSION: COATING MICROSTRUCTURE AND PROPERTIES

A. Microstructural Evolution and Defect Reduction

Scanning electron microscopy analysis revealed significant microstructural differences between the neat epoxy coating and graphene-reinforced variants, particularly regarding porosity and structural homogeneity. The neat epoxy coating exhibited numerous surface micropores and internal cavities, with crosssectional imaging showing voids up to 20 m in diameter distributed throughout the coating thickness. These defects originate from entrapped air between powder particles during deposition and insufficient flow during the melting and leveling stages of coating formation, creating direct pathways for corrosive species penetration.

The incorporation of graphene at 0.025 wt% loading substantially reduced both surface and internal porosity, with the coating surface showing a more continuous, homogeneous appearance and cross-sectional views revealing significantly fewer and smaller cavities. At higher magnification, individual graphene sheets could be observed bridging gaps between epoxy domains, suggesting a physical role in modifying the powder melting and coalescence behavior. The reduction in defect density correlates directly with improved barrier properties, as established through subsequent electrochemical testing.

The mechanism underlying this microstructural improvement appears to involve multiple factors. First, the graphene powder particles occupy spaces between the larger epoxy powder particles during electrostatic deposition, reducing the volume fraction of entrapped air. Second, during the heating stage, the high thermal conductivity of graphene facilitates more uniform heat distribution throughout the coating thickness, promoting simultaneous melting and improved flow characteristics. Third, the graphene sheets may physically reinforce the molten epoxy against bubble formation and coalescence during crosslinking.

At the highest graphene loading of 0.05 wt%, some reagglomeration became evident through the appearance of localized graphene-rich regions, though these did not produce the large-scale defects observed in the neat epoxy coating. This observation suggests that there exists an optimal loading range between 0.025 and 0.05 wt% where the benefits of graphene incorporation are maximized while avoiding the detrimental effects of agglomeration. The microstructural evidence supports the concept that ultralow graphene loadings can significantly influence coating formation processes through both physical and chemical mechanisms.

B. Thermal Behavior and Curing Characteristics

Differential scanning calorimetry provided insights into how graphene influences the thermal transitions and curing behavior of the epoxy powder system. All formulations exhibited two primary thermal events: an endothermic melting transition between 50-100°C and an exothermic curing reaction between 90-200°C. The melting behavior showed subtle but consistent changes with graphene incorporation, with the $Gr_{0.025}$/EP formulation exhibiting a slightly sharper melting endotherm and earlier onset temperature compared to the neat epoxy.

Analysis of the melting endotherm slopes according to established thermal conductivity models indicated a approximately 8% increase in effective thermal conductivity for the $Gr_{0.025}$/EP formulation compared to neat epoxy. This enhancement, while modest in absolute terms, appears sufficient to promote more uniform heating during the critical melting stage, reducing thermal gradients that can lead to uneven flow and defect formation. The improved heat distribution likely contributes to the observed reduction in coating porosity and more homogeneous microstructure.

The curing behavior showed more pronounced graphenedependent effects, with the $Gr_{0.025}$/EP formulation exhibiting a 3°C reduction in curing onset temperature (96.5°C vs. 99.5°C for neat epoxy) and a slight increase in reaction enthalpy (38.79 J/g vs. 37.23 J/g). This catalytic effect may originate from the surface-adsorbed PVA molecules, whose hydroxyl groups can participate in the epoxide ring-opening reactions, or from the graphene surfaces themselves providing nucleation sites for crosslinking initiation. The enhanced curing efficiency contributes to more complete network formation, reducing the concentration of unreacted sites that can absorb water and facilitate corrosion.

In contrast, the $Gr_{0.05}$/EP formulation showed a higher curing onset temperature (101.2°C) and significantly reduced reaction enthalpy (30.21 J/g), suggesting that at this higher loading, the physical barrier effect of graphene sheets begins to hinder molecular mobility and crosslinking reactions. This transition from catalytic to inhibitory behavior with increasing graphene content highlights the importance of optimizing nanofiller loading to achieve balanced processing and performance characteristics.

V. RESULTS AND DISCUSSION: ELECTROCHEMICAL PERFORMANCE

A. Impedance Spectroscopy and Barrier Properties

Electrochemical impedance spectroscopy measurements over 30-day immersion periods provided quantitative assessment of the corrosion protection performance evolution for all coating formulations. The neat epoxy coating exhibited relatively low initial impedance values (approximately 10^5 Ω·cm^2 at 0.01 Hz) that decreased steadily throughout the immersion period, reaching approximately 10^4 Ω·cm^2 after 30 days. This behavior reflects the inherent permeability of the epoxy matrix and the presence of microstructural defects that provide rapid pathways for electrolyte penetration.

All graphene-reinforced coatings showed significantly improved impedance characteristics, with the $Gr_{0.025}$/EP formulation demonstrating exceptional performance. This coating maintained impedance values above 10^7 Ω·cm^2 after 21 days immersion and approximately $10^{5.8}$ Ω·cm^2 after 30 days, representing one and two orders of magnitude improvement over the neat epoxy coating at these time points, respectively. The sustained high impedance indicates effective barrier function preservation even during extended exposure to aggressive chloride environments.

Equivalent circuit modeling quantified the evolution of coating resistance (R_c) and charge transfer resistance (R_{ct}) parameters, providing mechanistic insights into the protection mechanisms. The $Gr_{0.025}$/EP coating exhibited R_c values exceeding 10^{10} Ω·cm^2 initially and maintaining 10^5 Ω·cm^2 after 30 days, while R_{ct} values remained above 10^6 Ω·cm^2 throughout the testing period. These parameters confirm that the coating itself provides substantial resistance to ionic conduction while simultaneously limiting electrochemical activity at the coating-steel interface.

The appearance of Warburg diffusion impedance in the equivalent circuit models for graphene-reinforced coatings after 14-21 days immersion indicates that the protection mechanism transitions from pure barrier protection to limited diffusion control as electrolyte gradually penetrates the coating. This delayed onset of detectable interfacial activity further confirms the enhanced barrier properties imparted by graphene incorporation, particularly at the optimal 0.025 wt% loading.

B. Polarization Behavior and Corrosion Kinetics

Tafel polarization measurements after 30 days immersion provided complementary information about corrosion processes at the coating-steel interface. The neat epoxy coating exhibited a corrosion potential of -0.19 V vs. Ag/AgCl and corrosion current density of 2.31×10^{-6} A/cm^2, indicating active corrosion conditions with limited protective capability after extended exposure.

All graphene-reinforced coatings showed improved corrosion parameters, with the $Gr_{0.025}$/EP formulation demonstrating the most favorable characteristics: a noble shift in corrosion potential to 0.17 V vs. Ag/AgCl and reduced corrosion current density of 5.19×10^{-7} A/cm^2. This combination indicates both thermodynamic stabilization of the interface and kinetic

inhibition of corrosion reactions, consistent with effective barrier function and limited electrolyte access to the steel substrate.

The corrosion protection mechanism appears to involve both extended diffusion pathways due to the tortuosity effect of graphene sheets and reduced coating porosity limiting bulk electrolyte penetration. Additionally, the more complete crosslinking evidenced by DSC analysis may contribute to reduced water absorption and swelling, further preserving coating integrity during immersion. The optimal performance at 0.025 wt% loading suggests that a percolating network is not necessary for significant improvement, with well-dispersed individual sheets providing sufficient barrier enhancement at ultralow concentrations.

TABLE II: Electrochemical Parameters from EIS and Tafel Measurements After 30 Days Immersion

Sample	—Z—0.	01Hz 2 2 2Rc	Rct	icorr
	(Ω·cm)	(Ω·cm)	(Ω·cm)	(A/cm^2)
EP	2.62×10^4	4.08×10^4	2.62×10^4	2.31×10^{-6}
Gr0.0125/EP	2.11×10^5	4.92×10^4	2.11×10^5	8.13×10^{-7}
Gr0.025/EP	6.31×10^5	7.00×10^5	2.38×10^5	5.19×10^{-7}
Gr0.05/EP	7.65×10^4	4.46×10^4	7.65×10^4	9.19×10^{-7}

VI. RESULTS AND DISCUSSION: ADHESION AND DURABILITY PERFORMANCE

A. Interfacial Adhesion and Mechanical Integrity

Pull-off adhesion testing provided critical insights into the coating-substrate interface quality and its evolution during corrosive exposure. All coating formulations exhibited excellent initial adhesion strengths of approximately 4 MPa, consistent with the intrinsic adhesion characteristics of epoxy resins to steel substrates. This robust initial bonding establishes a foundation for long-term protection by limiting underfilm corrosion propagation through interfacial disbondment.

After 240 hours of salt spray exposure, significant differences emerged between the formulations. The neat epoxy coating showed substantial adhesion degradation, with bond strength reduced to approximately 1.5 MPa and evident interfacial failure modes. In contrast, the graphene-reinforced coatings maintained higher adhesion retention, with the $Gr_{0.025}$/EP formulation exhibiting the highest post-exposure adhesion strength of 3.88 MPa and predominantly cohesive failure within the coating layer.

The adhesion preservation mechanism likely involves multiple factors. First, the reduced coating porosity limits electrolyte accumulation at the coating-steel interface, minimizing the conditions for cathodic delamination. Second, the improved crosslinking density may enhance coating stiffness and reduce swelling stresses during water absorption. Third, the graphene sheets may physically reinforce the interface region through mechanical interlocking and stress distribution effects.

The adhesion performance correlates directly with the observed electrochemical behavior, as coatings maintaining strong interfacial bonds effectively limit the lateral spread of corrosion from defects and scratches. This synergy between barrier properties and adhesion retention represents a key advantage of the graphene-reinforced system, particularly for long-term service in aggressive environments where coating integrity at defects determines overall protection lifetime.

B. Salt Spray Resistance and Defect Tolerance

Accelerated salt spray testing provided visual evidence of corrosion protection performance under simulated severe service conditions. All coatings developed rust at intentionally introduced scratches within 48 hours of exposure, as expected when the steel substrate is directly exposed to the corrosive environment. However, significant differences emerged in the propagation of corrosion from these defects and the general surface condition over extended exposure.

The neat epoxy coating exhibited extensive rust staining emanating from scratches after 168 hours, with corrosion products accumulating significantly at defect sites and evidence of underfilm corrosion extending several millimeters from the scratch edges. This behavior indicates poor barrier function and limited resistance to interfacial corrosion propagation, consistent with the microstructural observations of high porosity.

The graphene-reinforced coatings showed progressively improved performance with increasing loading up to 0.025 wt%, with the optimal formulation exhibiting minimal corrosion propagation from scratches and no evidence of general surface deterioration. The reduced porosity and enhanced crosslinking likely contribute to this improved defect tolerance by limiting electrolyte penetration through the coating bulk and along the coating-substrate interface.

At the highest graphene loading (0.05 wt%), some localized blistering appeared near scratch edges after 168 hours, suggesting that excessive graphene content may create interfacial stress concentrations or minor aggregation sites that compromise coating integrity under wet conditions. This observation further supports the existence of an optimal composition window for balanced performance characteristics.

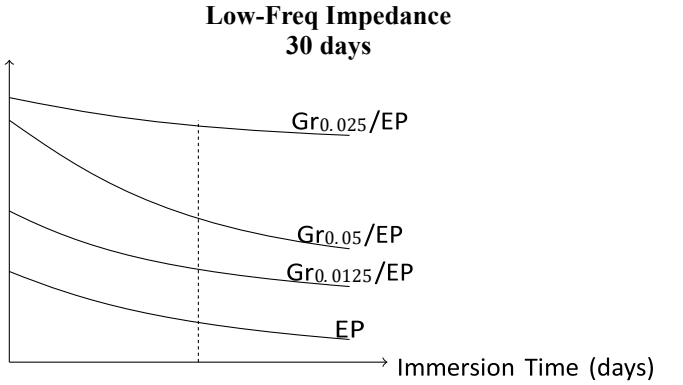

Fig. 2: Schematic representation of low-frequency impedance evolution during prolonged immersion, illustrating superior barrier maintenance by the optimally loaded graphene coating.

VII. CONCLUSIONS AND IMPLEMENTATION PERSPECTIVES

This comprehensive investigation establishes defect-sparse graphene as a highly effective nanoadditive for enhancing the performance of epoxy powder coatings through multiple complementary mechanisms. The liquid-phase shear exfoliation production method successfully yielded high-quality graphene with minimal structural defects, while the non-covalent PVA stabilization ensured compatibility with the epoxy matrix and facilitated uniform dispersion at ultralow loadings. The optimized coating formulation containing 0.025 wt% graphene demonstrated exceptional corrosion protection performance, maintaining impedance values above 10^7 Ω·cm^2 after 21 days immersion in 3.5% NaCl solution and preserving strong adhesion after aggressive salt spray exposure.

The reinforcement mechanism involves a complex interplay of microstructural, thermal, and chemical effects rather than a single dominant factor. Graphene incorporation reduced coating porosity by approximately 60% compared to neat epoxy, primarily through improved heat transfer during melting and physical bridging of powder particles during coalescence. The catalytic effect on curing reactions promoted more complete crosslinking, while the two-dimensional geometry created tortuous diffusion pathways that delayed electrolyte penetration. These combined effects produced synergistic improvements in barrier properties, adhesion retention, and overall corrosion protection performance.

The identification of an optimal loading range between 0.025 and 0.05 wt% highlights the importance of balanced formulation design, as excessive graphene content can lead to aggregation and processing challenges that offset the performance benefits. This ultralow effective loading makes the technology economically viable for industrial implementation while maintaining the environmental advantages of powder coating systems through elimination of solvent emissions and reduction of material usage.

Future development directions should explore the integration of additional functionalities through hybrid nanomaterial systems, such as combining graphene with inhibitor-loaded nanocontainers for self-healing capabilities or with conductive polymers for active corrosion protection. Scale-up considerations should address the consistency of graphene production at industrial volumes and the optimization of mixing processes for uniform nanomaterial distribution in powder formulations. The fundamental understanding of structure-property relationships established in this work provides a foundation for designing next-generation protective coating systems with tailored performance characteristics for specific application environments.

REFERENCES

[1] M. Nazari, Y. Zhang, A. Mahmoodi, G. Xu, J. Yu, J. Wu, and X. Shi, “Nanocomposite organic coatings for corrosion protection of metals: a review of recent advances,” *Progress in Organic Coatings*, vol. 163, p. 106573, 2022.

[2] N. Ayrillini, “A review on electrostatic powder coatings for the furniture industry,” *International Journal of Adhesion and Adhesives*, vol. 113, p. 103062, 2022.

[3] S. Kugler, P. Ossewicz-Rupniewska, E. Wierzhicka, and J. Lopinski, “Anhydride-cured epoxy powder coatings from natural-origin resins, hardeners, and fillers,” *Coatings*, vol. 11, no. 5, p. 531, 2021.

[4] F.-L. Jin, X. Li, and S.-J. Park, “Synthesis and application of epoxy resins: a review,” *Journal of Industrial and Engineering Chemistry*, vol. 29, pp. 1–11, 2015.

[5] W. Liu, R. Zhou, H. Goh, S. Huang, and X. Lu, “From waste to functional additive: toughening epoxy resin with lignin,” *ACS Applied Materials & Interfaces*, vol. 6, no. 8, pp. 5810–5817, 2014.

[6] P. Wang, D. Cai, and J. Liu, “Preparation of graphene-modified anticorrosion coating and study on its corrosion resistance mechanism,” *International Journal of Photoenergy*, vol. 2020, p. 8846644, 2020.

[7] A. Kuang, “Performance of corrosion protective epoxy blends-based nanocomposite coatings: a review,” *Polymer-Plastics Technology and Materials*, vol. 59, no. 6, pp. 658–673, 2019.

[8] U. Samad, M. Alam, A. Anis, H. Abdo, H. Shaikh, and S. Al-Zahrani, “Nanomechanical and electrochemical properties of zno-nanoparticlefilled epoxy coatings,” *Coatings*, vol. 12, no. 3, p. 282, 2022.

[9] Y. Xia, Y. He, C. Chen, Y. Wu, and J. Chen, “Mos2 nanosheets modified sio2 to enhance the anticorrosive and mechanical performance of epoxy coating,” *Progress in Organic Coatings*, vol. 132, pp. 316–327, 2019.

[10] S. Pourhashem, E. Ghasemy, A. Rashidi, and M. Vaezi, "A review on application of carbon nanostructures as nanofiller in corrosion-resistant organic coatings," *Journal of Coatings Technology and Research*, vol. 17, no. 1, pp. 19–55, 2019.
[11] J. Bunch, S. Verbridge, J. Alden, A. van der Zande, J. Parpia, H. Craighead, and P. McEuen, "Impermeable atomic membranes from graphene sheets," *Nano Letters*, vol. 8, no. 8, pp. 2458–2462, 2008.
[12] V. Berry, "Impermeability of graphene and its applications," *Carbon*, vol. 62, pp. 1–10, 2013.
[13] R. Zhang, X. Yu, Q. Yang, G. Cui, and Z. Li, "The role of graphene in anti-corrosion coatings: a review," *Construction and Building Materials*, vol. 294, p. 123613, 2021.
[14] J. Li, H. Zheng, L. Liu, F. Meng, Y. Cui, and F. Wang, "Modification of graphene and graphene oxide and their applications in anticorrosive coatings," *Journal of Coatings Technology and Research*, vol. 18, no. 2, pp. 311–331, 2021.
[15] F. Andreatta, A. Rondinella, M. Zanocco, G. Capurso, R. Vendramin, A. Guarino, and L. Fedrizzi, "Corrosion, electrical and thermal behaviour of graphene modified polyester powder coatings," *Progress in Organic Coatings*, vol. 179, p. 107517, 2023.
[16] Z. Du, S. Wen, J. Wang, C. Yin, D. Yu, and J. Luo, "The review of powder coatings," *Journal of Materials Science and Chemical Engineering*, vol. 4, no. 5, pp. 4–9, 2016.
[17] J. Zhang, G. Kong, S. Li, Y. Le, C. Che, S. Zhang, D. Lai, and X. Liao, "Graphene-reinforced epoxy powder coating to achieve high performance wear and corrosion resistance," *Journal of Materials Research and Technology*, vol. 20, pp. 4148–4160, 2022.
[18] K. Paton, E. Varrla, C. Backes, R. Smith, U. Khan, A. O'Neill, C. Boland, M. Lotya, O. Istrate, P. King *et al.*, "Scalable production of large quantities of defect-free few-layer graphene by shear exfoliation in liquids," *Nature Materials*, vol. 13, no. 6, pp. 624–630, 2014.
[19] Z. Khanam, J. Liu, and S. Song, "High-concentration graphene dispersions prepared via exfoliation of graphite in pva/h2o green solvent system using high-shear forces," *Journal of Nanoparticle Research*, vol. 23, no. 6, p. 170, 2021.
[20] T. Guzel, "Investigation of the usability of extreme temperature changes¨ in pristine graphene production," *FlatChem*, vol. 26, p. 100223, 2021.
[21] D. Price and M. Jarratt, "Thermal conductivity of ptfe and ptfe composites," *Thermochimica Acta*, vol. 392, pp. 231–236, 2002.
[22] Y. Ye, D. Zhang, T. Liu, Z. Liu, W. Liu, J. Pu, H. Chen, H. Zhao, and X. Li, "Improvement of anticorrosion ability of epoxy matrix in stimulate marine environment by filled with superhydrophobic poss-go nanosheets," *Journal of Hazardous Materials*, vol. 364, pp. 244–255, 2019.
[23] U. Halim, C. Zheng, Y. Chen, Z. Lin, S. Jiang, R. Cheng, Y. Huang, and X. Duan, "A rational design of cosolvent exfoliation of layered materials by directly probing liquid-solid interaction," *Nature Communications*, vol. 4, no. 1, p. 2213, 2013.